International Journal Of
Industrial Electronics Control and Optimization
Print ISSN: 3517-2645
Online ISSN: 3568-2645
Homepage: https://ieco.usb.ac.ir/

Torque Vector Control and Direct Force Control in a Three-Phase Bearing-Less Induction Motor

Reza Ghanizadeh[1] | Hamed Azadrou[2] |

[1]Department of Electrical Engineering, Urmia Branch, Islamic Azad University, Urmia, Iran.
[2]Department of Electrical Engineering, Salmas Branch, Islamic Azad University, Salmas, Iran.
Corresponding author's email: azadrou.elec@gmail.com

Article Info

Article type:
Research Article

Article history:
Received: 28-May-2024
Received in revised form: 22-September-2024
Accepted: 15-October-2024
Published online: 22-June-2025

Keywords:
Bearing-less motor,
Torque control,
Levitation force control,
Vector control,
Direct force control.

ABSTRACT

Bearing-less induction motors (BLIMs) are suitable candidates for high-speed applications but suffer from low torque density and complex control issues due to the interaction of torque and levitation forces. To address these challenges, this paper presents a new control strategy that combines vector control and direct torque control (DTC) for torque management, alongside a novel force control method based on finite element analysis (FEA). The proposed approach minimizes interference between torque and force magnetic fields by employing a parallel winding structure and distinct control units for torque and force. Simulation results demonstrate that the proposed method significantly reduces torque ripple and improves steady-state performance compared to conventional vector control and DTC. Furthermore, the force control unit outperforms a dual field-oriented control (FOC) method in regulating rotor position, offering better suspension force control and faster stabilization. This work contributes to the development of more efficient control strategies for BLIMs, enhancing their performance in industrial applications.

NOMENCLATURE

W_m	Magnetic energy	L_{2s}	Torque windings self-inductances
i_{ab}	Two-phase current vector	L_{4s}	Force windings self-inductances
L_{ab}	Inductance matrix	F_{av}	Average suspension force
F_x and F_y	Suspension forces in x and y directions	T_{av}	Average electromagnetic torque
ω_{rm}	Mechanical rotor speed	$\psi_{2\alpha r}, \psi_{2\beta r}$	Flux linkages
ω_{2s}	Two pole slip frequency	v_k	Terminal voltage vector
ω_{4s}	Four pole slip frequency	i_k	Winding current vector
$i_{2\alpha s}, i_{2\beta s}$	Two pole stator constant dc currents	ψ_k	Flux linkage vector
$i_{2\alpha r}, i_{2\beta r}$	Two pole rotor constant dc currents	L	Inductance matrix
$i_{4\alpha s}, i_{4\beta s}$	Four-pole stator constant dc currents	γ	Angle between stator and rotor fluxes
$i_{4\alpha r}, i_{4\beta r}$	Four pole rotor constant dc currents	n_{1p}	Number of pole pairs in torque windings
M'_{24}	Mutual inductance between torque and force windings		

I. Introduction

Bearing-less motors are attractive electrical machines that work without any mechanical connection between the stationary and moving parts. This offers advantages such as low thermal problems, low maintenance requirements, high-speed capability, and no spark [1]. The stator in a bearing-less induction motor is same as a conventional induction motor. But, two separate windings are located in each slot which are connected to distinct power supplies. Fist P pole winding called torque or motoring winding which generates the torque electromagnetic field. The second one, is P±2 pole force winding which generates the suspension force field [2-5]. Despite the simplicity of this structure, the torque density is very low, which is due to the occupation of the slot space

by the force winding. The combined winding structure partially solves the problem and enhances the efficiency as much as conventional induction motors. In this method both fields are produced by a single set of windings [6-8]. However, the combined winding strategy requires a complicated power electronics converter constructed. Moreover, there is speed induced voltage in force windings which reduces the quality of performance, especially at high speeds.

The motor proposed in this work, has been designed and manufactured based on a novel winding strategy presented in [9] and [10]. The structure consists of two three phase parallel coils, one of which has a neutral point, while the other is connected to the force power supply. Researches have shown that parallel winding structure can reduce the speed induced voltage in the force windings to zero.

Control of a BLIM is an inherently challenging problem due to the effect of rotor induced currents. In addition to the torque current, force current is also induced in the rotor bars which degrade the torque and force quality. Also, the magnetic suspension force is defined with respect to displacement and current. So, the transfer function is unstable complicating the controller design. Vector control in a bearing-less motor with combined winding structure has been explained in [11]. In [12], a non-linear control system for an especial type bearing-less motor with rotor angle consideration has been presented. Fuzzy logic systems have been used in some articles to control the rotor position [13] and [14]. This method is usually fast and does not require complex mathematical equations. Among the other methods that can be used for estimating the parameters of an induction motor in control methods is the PSO algorithm [15]. Accurate estimation of the induction motor parameters has a significant impact on the performance and quality of the control system. The effects of cross-coupling in a combined winding BM by extracting an appropriate disturbance transfer function has been investigated in [16]. Decouple and separate control of the torque and force windings voltage disturbances is the most important point in a bearing-less motor. [17] investigated a DPNV type bearing-less motor and has shown that the structure is very effective in the field interference reduction. Optimization of the commutation period in a bearing-less motor has been proposed in [18]. In the work, the turn- on angle and conduction region of each phase winding have been chosen as the control targets.

In this work, a new control strategy has been provided for a BLIM. Force control unit is based on finite element analysis without any need to complex mathematical equations. Torque control unit is a modified direct torque control method based on phase currents controllers.

II. Proposed BLIM

A. Structure of the motor

Traditional BLIMs consist of two separate windings located in same slots which create torque field and force field. In combined winding structure, both fields are generated by only one winding set. But the existence of non-zero speed induced voltage in the force windings significantly reduces the system efficiency. To solve the problem, a parallel winding structure has been used which is shown in Fig. 1.

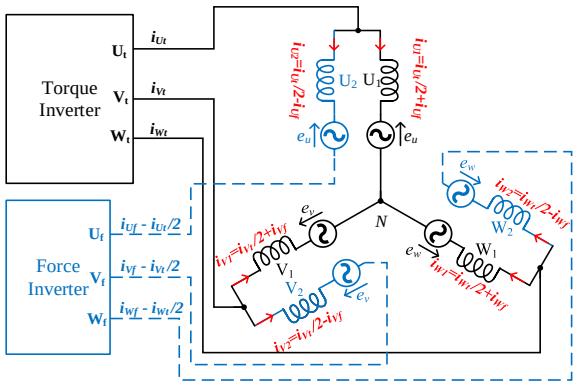

Fig. 1. BLIM with parallel winding structure

This structure has two sets of terminals, one for torque current and the other for suspension force current. Although both terminals belong to the common coil, the torque terminal is connected in such a way that the two similar parts of the coil have opposite directions. The winding of phase k (k=u, v, w) has two parallel parts denoted by k_1 and k_2 in Fig. 1, one is connected to the neural point point and the other one is connected to the force inverter. The current of phase k of the torque winding is divided between two parts k_1 and k_2, so that half of the current enters each of coils and induces the speed voltage (e_k) in them. The force inverter supplies current $(i_{kt}/2 - i_{kf})$ into the winding, where the force current i_{kf} flows through both coils k_1 and k_2. The speed induced voltage in one of the force windings is negative while the other winding has a positive induced voltage, so that eventually the windings will be without voltage. In this way, the force current can be controlled independently of the rotor speed and without the need for isolation with the torque inverter.

B. Dynamic equations

Terminal voltage in the torque and force inverters consists of three components including the resistance drop voltage, the electromotive force, and the speed voltage.

$$v_k = R_k i_k + L\frac{di_k}{dt} + \omega\frac{d\psi_k}{dt} \quad (1)$$

where the bold parameters v_k. i_k. and ψ_k represent the windings voltage vector, windings current vector, and flux linkage vector, respectively.

$$v_k = \begin{bmatrix} v_{U1} \\ v_{U2} \\ v_{V1} \\ v_{V2} \\ v_{W1} \\ v_{W2} \end{bmatrix},\ i_k = \begin{bmatrix} i_{U1} \\ i_{U2} \\ i_{V1} \\ i_{V2} \\ i_{W1} \\ i_{W2} \end{bmatrix}, \text{and } \psi_k = \begin{bmatrix} \psi_{U1} \\ \psi_{U2} \\ \psi_{V1} \\ \psi_{V2} \\ \psi_{W1} \\ \psi_{W2} \end{bmatrix}, \quad (2)$$

And L denotes the self and mutual inductances in a 6×6 matrix as follows.

$$L = \begin{bmatrix} L_u & M_{11} & M_{12} & M_{13} & M_{12} & M_{13} \\ M_{11} & L_u & M_{13} & M_{12} & M_{13} & M_{12} \\ M_{12} & M_{13} & L_v & M_{11} & M_{12} & M_{13} \\ M_{13} & M_{12} & M_{11} & L_v & M_{13} & M_{12} \\ M_{12} & M_{13} & M_{12} & M_{13} & L_w & M_{11} \\ M_{13} & M_{12} & M_{13} & M_{12} & M_{11} & L_w \end{bmatrix} \quad (3)$$

where, M_{11} denotes the mutual inductance between two coils $k_1$and k_2, M_{12} is the mutual inductance between coil k_1 and $k_2{}'$, M_{13} illustrates the mutual inductance between coil k_1 and $k_3{}'$, and L_k denotes the self inductance of winding k, while $L_u = L_v = L_w = L$.

Considering $R_k = R$ and according to the matrixes, the voltage in terminals u_1 and u_2 are written as:

$$v_{u_1} = R\left(\frac{i_{ut}}{2} + i_{uf}\right) + \frac{1}{2}(L + M_{11} - M_{12} - M_{13})\frac{di_{ut}}{dt} + (L - M_{11} - M_{12} + M_{13})\frac{di_{uf}}{dt} + \omega\frac{d\psi_u}{dt} \quad (4)$$

$$v_{u_2} = R\left(\frac{i_{ut}}{2} - i_{uf}\right) + \frac{1}{2}(L + M_{11} - M_{12} - M_{13})\frac{di_{ut}}{dt} - (L - M_{11} - M_{12} + M_{13})\frac{di_{uf}}{dt} + \omega\frac{d\psi_u}{dt} \quad (5)$$

According to Fig. 1, the terminal voltage of the force converter can be calculated as:

$$v_{u_f} = v_{U_1} - v_{U_2} = 2R.i_{uf} + 2(L - M_{11} - M_{12} + M_{13})\frac{di_{uf}}{dt} \quad (6)$$

Same equations can be written for two other phases. The equation indicates that voltage of the force winding is independent of the speed induced component.

III. Control of BLIM

There are different factors that affect a BLIM performance. A delay in force response of a BLIM is one of them, which can be caused by iron losses, saturation, etc. Another factor is the error of the angular position of the rotor, which is caused by the interference of suspension force in axes x and y. Also, the interference between the torque and force fields is very important in suspension system performance in a BLIM. The motor proposed in this work has been constructed with the special structure explained in the previous section which almost eliminates the interference between the electromagnetic fields. Due to the non-linear structure, mathematical model can't guarantee the precise performance of the BLIM, especially at high speeds. In order to compensate the direction error and the delay in suspension force generation system, a new method has been proposed in this work which is based on finite element analysis (FEA) of the motor. In the presented control method, all non-linear working conditions of the motor are taken into account in FEA, and there is no need for complicated and time-consuming mathematical equations in force control unit. Moreover, a new torque control strategy including a switching table and current controller has been proposed that shows a precise and fast responses.

A. Proposed Force Control Strategy

In the proposed system, the data obtained by finite element analysis are used to model the system. Therefore, there is no need to use complex and high-order equations. Fig. 2 shows some rotor displacements from the center and the appropriate compensating force vectors. It can be seen that without any deviation, there is only a constant force F_0 in vertical direction to suspend the rotor.

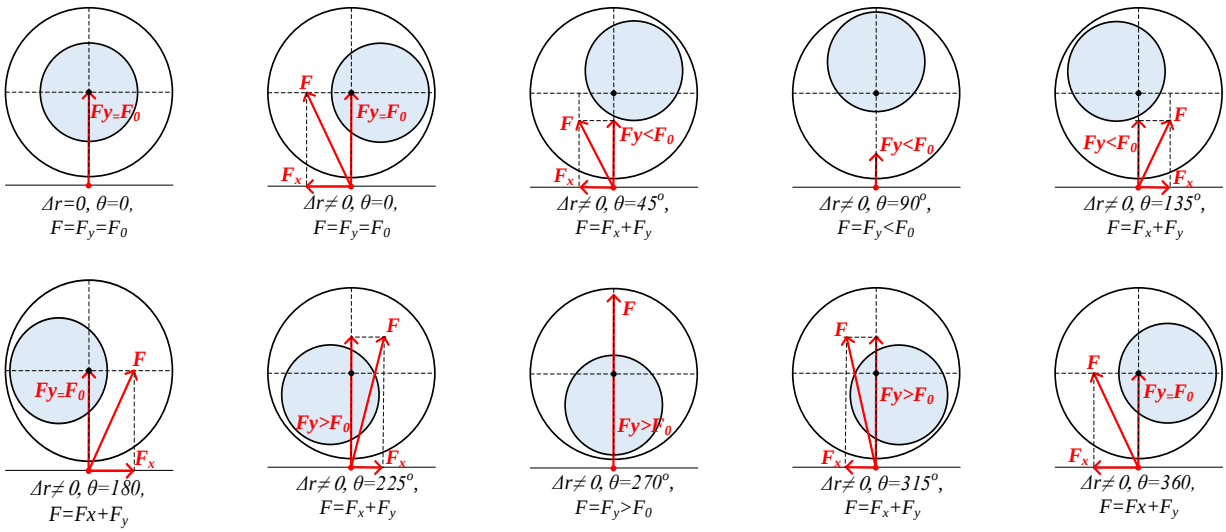

Fig. 2. Rotor deviation in different directions and suspension force vector

By defining Δr as the deviation of the rotor from the center and θ as the counterclockwise deviation angle from the horizontal axis, at the first step the suspension force vector $\vec{F} = F_x + F_y$ is determined for the command position of the rotor $\Delta r = 0$ and $\theta = 0$. In the following, the force factor is obtained for $\theta = 0$, and $\Delta r = 0.2.0.4 \ldots \ldots 2$ mm. The step is repeated exactly for $\theta = 5.10. \ldots .360$ and the corresponding force values are recorded. In this way, a set of data has been obtained that show the relationship between the force and the deviation from the center of the rotor in the entire movement range.

By defining Δr as the deviation of the rotor from the center and θ as the counterclockwise deviation angle from the horizontal axis, at the first step the suspension force vector $\vec{F} = F_x + F_y$ is determined for the command position of the rotor $\Delta r = 0$ and $\theta = 0$. In the following, the force factor is obtained for $\theta = 0$, and $\Delta r = 0.2\ 0.4 \ldots \ldots 2$ mm. The step is repeated exactly for $\theta = 5.10. \ldots .360$ and the corresponding force values are recorded. In this way, a set of data has been obtained that show the relationship between the force and the deviation from the center of the rotor in the entire movement range. By using curve fitting technique, the above relationship is made continuous covering all points of the air gap. The obtained profile for the proposed BLIM is shown in Fig. 3. Further investigations shown that the profiles are independent of the load torque value.

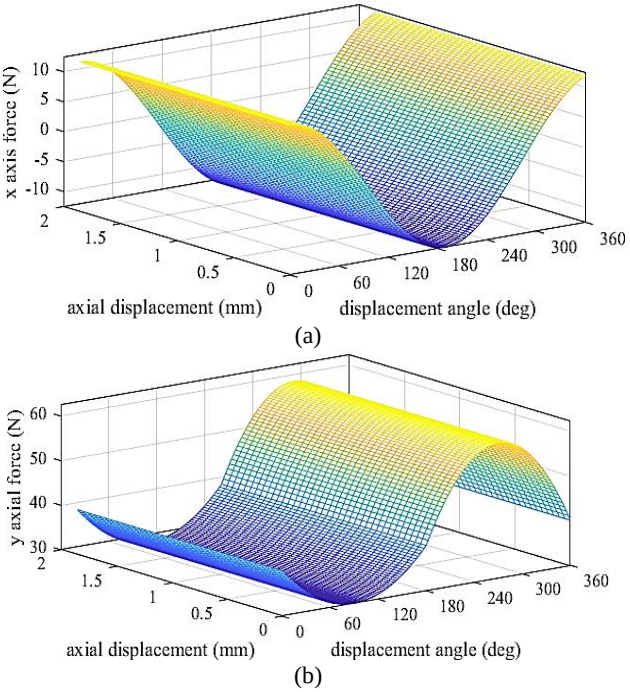

Fig. 3. Data obtained by FEA for the proposed BLIM

The data obtained by FEA are used to extract the suspension force vector for each deviation of rotor from the center. Block diagram of the proposed force control system is shown in Fig. 4.

As deviation of the rotor is determined by the position sensors, parameters Δr and θ are calculated and entered into the FEA block. This block is the continuous form of Fig. 3, which, selects the values F_x^* and F_y^* for a specified load torque. Assuming that the stator and rotor currents are specified by *s* and *r*, the suspension force in a squirrel cage BLIM has been illustrated in [19] as a matrix equation.

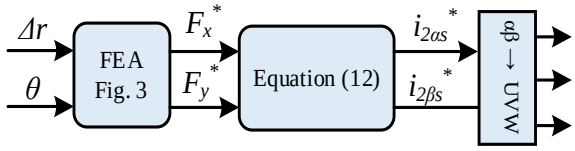

Fig. 4. Force control system

$$\begin{bmatrix} F_x \\ F_y \end{bmatrix} = M' \begin{bmatrix} i_{1\alpha g} & i_{1\beta g} \\ -i_{1\beta g} & i_{1\alpha g} \end{bmatrix} \begin{bmatrix} i_{2\alpha g} \\ i_{2\beta g} \end{bmatrix} \quad (7)$$

$$\begin{cases} i_{2\alpha g} = i_{2\alpha s} + i_{2\alpha r} \\ i_{2\beta g} = i_{2\beta s} + i_{2\beta r} \end{cases} \quad (8)$$

where M' is a parameter related to the motor dimensions and characteristics, calculated as [19]. Numbers 1 and 2 in parameters correspond to the torque and force windings current, respectively. Also, α and β are axes in the two phases system. For example, $i_{1\alpha g}$ and $i_{2\alpha g}$ denote the airgap flux component of current in torque and force windings, respectively. The BLIM proposed in this work has a special rotor structure presented in [4]. This structure has a main advantage that no current is induced by the stator force currents on the rotor. This means $i_{2\alpha r} = i_{2\beta r} = 0$, and so, $i_{2\alpha g} = i_{2\alpha s}$ and $i_{2\beta g} = i_{2\beta s}$. In this way, the suspension force will be proportional to the torque winding current.

$$i_{2\alpha s} = \frac{F_x^*}{M'.I_m} = k_f F_x^* \text{ and } i_{2\beta s} = \frac{F_y^*}{M'.I_m} = k_f F_y^* \quad (9)$$

This is an assumption that greatly simplifies the analysis. But the study on the BLIM and its control system showed that the use of exact motor equations leads to a better response and compensates the delay. Flux linkages in the two-phase system can be expressed as:

$$\begin{cases} \psi_{2\alpha r} = L_u \times i_{2\alpha r} + M_2 \times i_{2\alpha s} \\ \psi_{2\beta r} = L_u \times i_{2\beta r} + M_2 \times i_{2\beta s} \end{cases} \quad (10)$$

where M_2 is the mutual inductance between the stator force winding and the rotor. By combining the equations (8) and (10), it may be written

$$\begin{cases} i_{2\alpha g} = i_{2\alpha s} + \frac{1}{L_u}(\psi_{2\alpha r} - M_2 i_{2\alpha s}) \\ i_{2\beta g} = i_{2\beta s} + \frac{1}{L_u}(\psi_{2\beta r} - M_2 i_{2\beta s}) \end{cases} \quad (11)$$

Also, in an airgap flux-oriented vector control method, the vertical current component is zero ($i_{1\beta g} = 0$). For a constant α axis current ($i_{2\alpha s}$=I_m), combination of (7) and (11) is:

$$\begin{cases} i_{2\alpha s} = \left(\frac{F_x^*}{M'.I_m} - \frac{\psi_{2\alpha r}}{L_u}\right) / \left(1 - \frac{M_2}{L_u}\right) \\ i_{2\beta s} = \left(\frac{F_y^*}{M'.I_m} - \frac{\psi_{2\beta r}}{L_u}\right) / \left(1 - \frac{M_2}{L_u}\right) \end{cases} \quad (12)$$

The complete block diagram of the BLIM control system is shown in Fig. 6.

The obtained two phase force winding currents are compared with the corresponding actual currents measured by sensors and the error is entered to a PI controller. Proportional and integral gains of this controller in this controller have been obtained based on trial-and-error method as 1.28 and 0.025, respectively.

B. Proposed Torque Control Strategy

Various vector control (VC) structures have been presented for induction motors in all of them the stator current is used to control the produced torque. Assuming that indices "1" show the values related to the torque windings, the current is decomposed into two perpendicular torque and flux components denoted by $i_{1\alpha}$ and $i_{1\beta}$, which are used to control the torque and flux, respectively. So, the torque in rotor flux reference frame can be written as

$$T_e = \frac{3}{2} n_{1p} \frac{L_{1m}}{L_r} \left(\psi_{1\alpha r} \times i_{1\beta r} - \psi_{1\beta r} \times i_{1\alpha r}\right) \quad (13)$$

where L_{1m} and L_r denote the magnetizing inductance and rotor inductance, respectively. n_{1p} is the number of pole pairs in the torque windings. Also, $\psi_{1\alpha r}$ and $\psi_{1\beta r}$ indicate two perpendicular axes rotor flux linkages. Ignoring the flux in α axis, it can be written as:

$$T_e = \frac{3}{2} n_{1p} \frac{L_{1m}}{L_r} \left(\psi_{1\alpha r} \times i_{1\beta r}\right) \quad (14)$$

On the other hand, a direct torque control (DTC) system does not require any current controller. The equations of a DTC for the torque windings of a BLIM can be written as:

$$T_e = \frac{3}{2} n_{1p} I_m\{\vec{\psi}_{1s}^{*}\, \vec{i}_{1s}\} \quad (15)$$

$$\vec{i}_{1s} = \frac{1}{\sigma L_{1s}} \vec{\psi}_{1s} - \frac{L_m}{\sigma L_{1s} L_r} \vec{\psi}_{1r}.\ \sigma = 1 - \frac{L_m^2}{L_{1s} L_r} \quad (16)$$

Combining the equations, following equation is obtained.

$$T_e = \frac{3}{2} n_{1p} \frac{L_m}{\sigma L_{1s} L_r} |\vec{\psi}_{1s}||\vec{\psi}_{1r}| sin\gamma \quad (17)$$

Where γ denotes the angle between the stator and rotor flux linkage vectors. The derivative of (17) indicates that, the produced torque depends on angle γ. Therefore, the motor torque can be controlled quickly by adjusting the angle γ. By applying appropriate voltage vectors to the stator torque windings, the phase equation for a torque winding on stator can be written as follows.

$$\frac{d\vec{\psi}_{1s}}{dt} = \vec{V}_{1s} - R_{1s}\vec{i}_{1s} \approx \vec{V}_{1s} \rightarrow \Delta\vec{\psi}_{1s} = \vec{V}_{1s}\Delta t \quad (18)$$

$$\frac{d\vec{\psi}_{1r}}{dt} + \left(\frac{L_m}{\sigma L_{1s} L_r} - \frac{R_r}{L_r} - j\omega_2\right)\vec{\psi}_{1r} = \frac{R_r L_m}{\sigma L_{1s} L_r}\vec{\psi}_{1s} \quad (19)$$

where indices "1" show the values related to the torque windings. In order to obtain a fast response with low ripple and high precision, a new control strategy has been presented in this work which includes a switching table instead of pulse width modulation (PWM) method. Also, hysteresis current controllers have been used to adjust the torque winding currents. Assuming that the flux is constant and Δ denotes small variation, the equations of the conventional vector control method in the torque windings can be written as:

$$\begin{cases} |\vec{\psi}_{1r}| = K_\alpha \times i_{1\alpha} \\ T_e = K_\beta \times i_{1\beta} \end{cases} \rightarrow \begin{cases} |\vec{\psi}_{1r}| \propto i_{1\alpha} \\ T_e \propto i_{1\beta} \end{cases} \rightarrow \begin{cases} \Delta|\vec{\psi}_{1r}| \propto \Delta i_{1\alpha} \\ \Delta T_e \propto \Delta i_{1\beta} \end{cases} \quad (20)$$

Based on direct torque control strategy, by applying a voltage in a short switching interval, the stator flux vector rotates from $\vec{\psi}_{1s}$ to $\vec{\psi}_{1s}^{1}$, as shown in Fig. 5. Due to the large time constant of the rotor, it can be assumed with reasonable accuracy that the rotor flux linkage is constant in this interval.

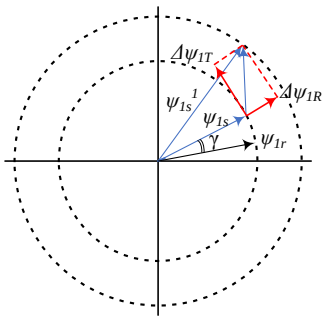

Fig. 5. Flux change in a short switching interval

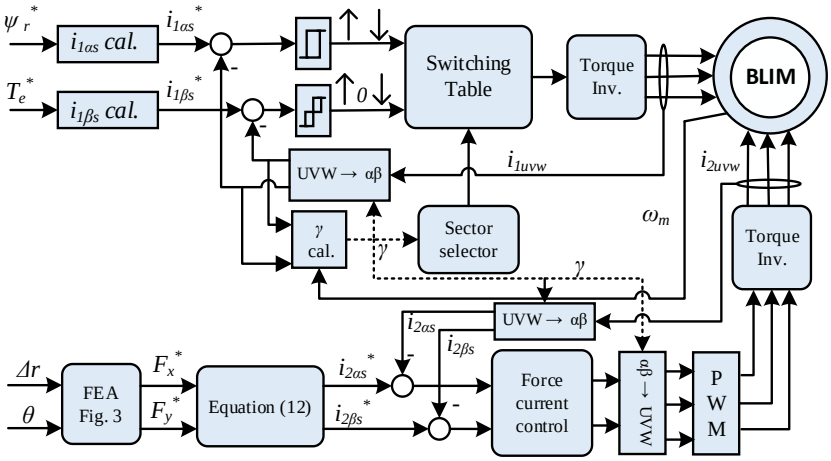

Fig. 6. Block diagram of the proposed control system for the BLIM.

Change of stator flux $\Delta\vec{\psi}_{1s}$ is decomposed into two radial and tangential components denoted by $\Delta\vec{\psi}_{1R}$ and $\Delta\vec{\psi}_{1T}$, respectively. According to Fig. 5, (17) can be rewritten as follows:

$$\Delta T_e = K\left|\vec{\psi}_{1r}\right|\left(\left|\vec{\psi}_{1s}^{1}\right|sin(\gamma+\Delta\gamma) - \left|\vec{\psi}_{1s}\right|sin\gamma\right) \quad (21)$$

With suitable approximations

$$sin(\gamma+\Delta\gamma) = sin\gamma + cos\gamma\ sin\Delta\gamma \quad (22)$$

$$sin\Delta\gamma = \frac{\Delta\vec{\psi}_{1T}}{\left|\vec{\psi}_{1s}\right|} \quad (23)$$

$$\left|\vec{\psi}_{1s}^{1}\right| = \left|\vec{\psi}_{1s}\right| + \Delta\vec{\psi}_{1T} \quad (24)$$

Equation (21) can be written as follows.

$$\Delta T_e = K\left|\vec{\psi}_{1r}\right|\left\{\Delta\psi_{1T}cos\gamma + \Delta\psi_{1R}\ sin\gamma + \frac{\Delta\psi_{1T}\,\Delta\psi_{1R}}{\left|\vec{\psi}_{1s}\right|}cos\gamma\right\} \quad (25)$$

Second and third terms are ignorable. Therefore, (25) can be simplified as:

$$\Delta T_e = K\left|\vec{\psi}_{1r}\right|\Delta\psi_{1T}\ cos\gamma \ \rightarrow\ \ \Delta T_e \propto \Delta\psi_{1T} \quad (26)$$

$$\Delta\left|\vec{\psi}_{1s}\right| = \Delta\psi_{1R} \quad (27)$$

Ignoring the first order delay between stator and rotor linkage fluxes in (19), it can be obtained

$$\Delta\left|\vec{\psi}_{r}\right| = \Delta\psi_{1R} \quad (28)$$

Comparing the equations (18), (26), and (28) gives the following results.

$$\Delta\psi_{1R} \propto \Delta i_{1\alpha} \quad (29)$$

$$\Delta\psi_{1T} \propto \Delta i_{1\beta} \quad (30)$$

According to the analysis, block diagram of the proposed control method is shown in Fig. 6. It can be seen that the proposed torque controller is a direct control method in which, unlike the conventional DTC, the phase currents are controlled. The obtained results show that this has a good effect on the performance quality with respect to the conventional DTC. On the other hand, PI controllers and PWM have been eliminated, which reduces the system response time with respect to the conventional vector control method. The proposed controller includes hysteresis controllers for the current components, like a vector control, and a switching table as a direct torque control strategy.

IV. Simulation Evaluation

In order to examine the performance of the proposed control system, the BLIM along with the control system have been simulated in Matlab/Simulink software. Parameters of the BLIM are shown in TABLE I. For a more complete study, the results obtained by the proposed controller are compared with the dual field oriented method [10]. The suspension force profile with respect to other parameters are shown in Fig. 7.

To evaluate the performance of the four-pole motoring unit, an external load has been applied to the motor at t= 0.8 s. The obtained results using conventional vector control (VC), direct torque control (DTC), and the proposed control system have been shown in Fig. 8. As mentioned in the previous section, the proposed system is a current controller system which works based on switching table. The results indicate that the torque resulted by proposed system has less ripple than the conventional DTC method, while its transit time is better than the VC.

TABLE 1 PARAMETERS OF THE PROTOTYPE BLIM

Parameter	Symbol	Constraints
Power	P	2200 W
Speed	N	15000 rpm
Torque winding poles	P_t	2
Force winding poles	P_f	4
Supply frequency	f	250 Hz
Stator slots	Q_s	30
Rotor slots	Q_r	24
Voltage	V_L	220 V
Torque winding phase current	I_t	10 A
Force winding phase current	I_s	5 A
Stack length	l	38 cm
Rotor slot depth	h_{rp}	2.5 cm
Stator slot fill factor	f_f	0.6

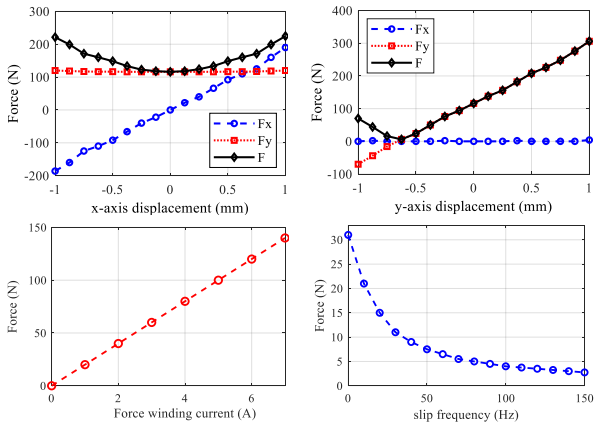

Fig. 7. Electromagnetic force in BLIM.

To show the force controller performance, it is assumed that the rotor is initially located at point $x = -0.2$ mm and $y = -0.1$ mm. As shown in Fig. 9, the electromagnetic forces are generated in two directions to return the rotor to the center of the stator. Fig. 9 (a) indicates the forces in the dual field-oriented control (FOC) presented in [11] while forces obtained by the proposed controller are shown in Fig. 9 (b). In both Fig. 9 (a) and Fig. 9 (b), the horizontal axis force (F_x) is produced for a short time and when the rotor

reaches the center, this force becomes zero. But the vertical force is reduced to a specified value to levitate the rotor in the center in normal performance condition. In this work, the displacement tolerance of the rotor in two directions is defined as 0.01 mm. In this way, after the rotor returns to this range, the force becomes zero. The rotor position variation in the process is shown in Fig. 9 (c) and (d) for the dual FOC and proposed system, respectively. The results indicate that using the proposed control system, the rotor returns to the center almost directly and in a short time.

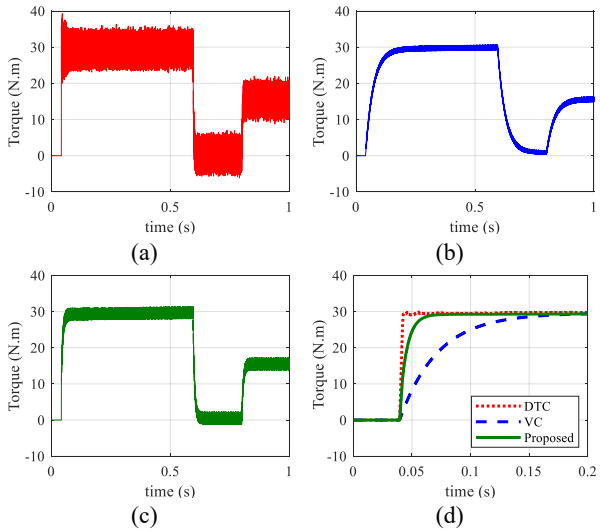

Fig. 8. Torque comparison, (a) direct torque control, (b) vector control, (c) proposed control, (d) transient time comparison.

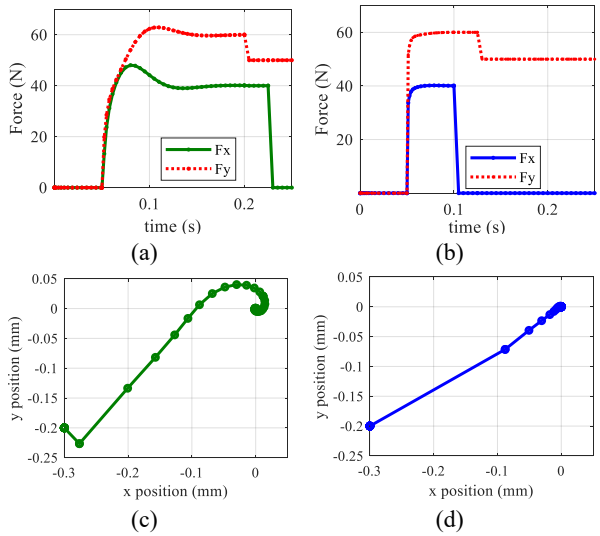

Fig. 9. Force comparison, (a) dual FOC method, (b) proposed method..

In order to investigate the rotor deviation in critical situations, an external load was applied to the motor at t=0.8 s and the results were extracted as Fig. 10. Comparison of position fluctuations using the dual FOC and the proposed controller confirm that the proposed force control method can regulate the suspension force so that the rotor has less fluctuations. To further demonstrate the effectiveness of the proposed control method, its performance on the bearingless induction motor has been compared with the method proposed in reference [20]. This comparison, under load conditions and during the moment of load application at t= 1.2 s, is shown in Fig. 11. This figure shows the currents with rotor deviation from the center. Fig. 11 (a) and (b) compare the force winding currents and Fig. (c) and (d) demonstrate the torque winding current of the motor using two control strategies. It can be observed that the proposed radial position control exhibits a short transient time during both startup and load application.

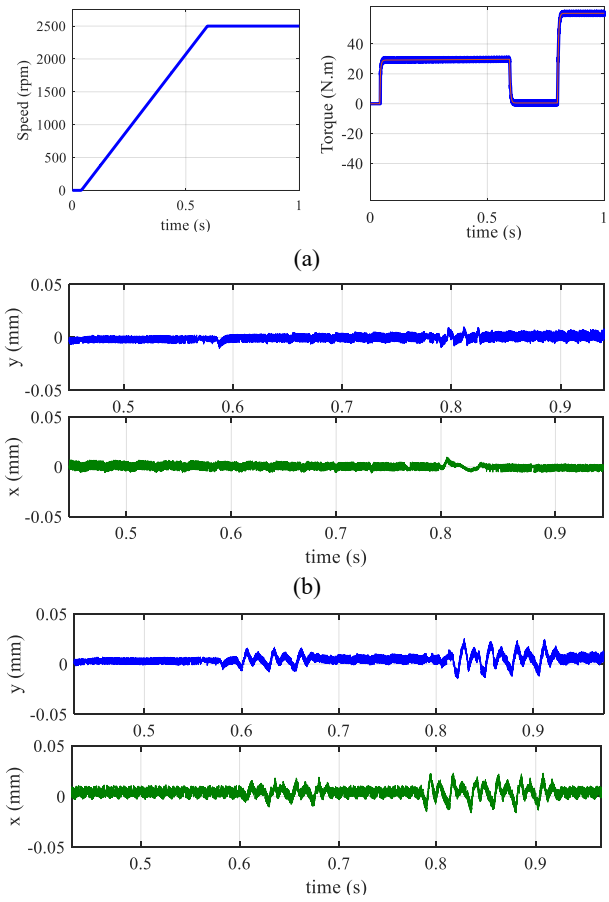

Fig. 10. Rotor position comparison, (a) speed and torque profiles, (b) proposed method, (c) dual FOC method.

V. Conclusions

A new control method for a parallel winding bearing-less induction motor has been presented. The method includes distinct torque and force control units. A direct torque control strategy with a current controller was used to adjust the motor torque and speed. The outputs obtained by the strategy is faster than conventional direct torque controller while includes fewer ripples in compare with conventional vector controller. Also, a new force control strategy was

presented that uses finite element analysis data to determine the appropriate force winding current. Using this method, the suspension force is adjusted without any complicated mathematical equations. The results obtained by simulation showed that the proposed control system shows acceptable capability in distinct control of torque and force in a bearing-less induction motor. The effect of load application on the force current is negligible using the proposed control strategy, and the rotor returns to the center position more quickly during startup.

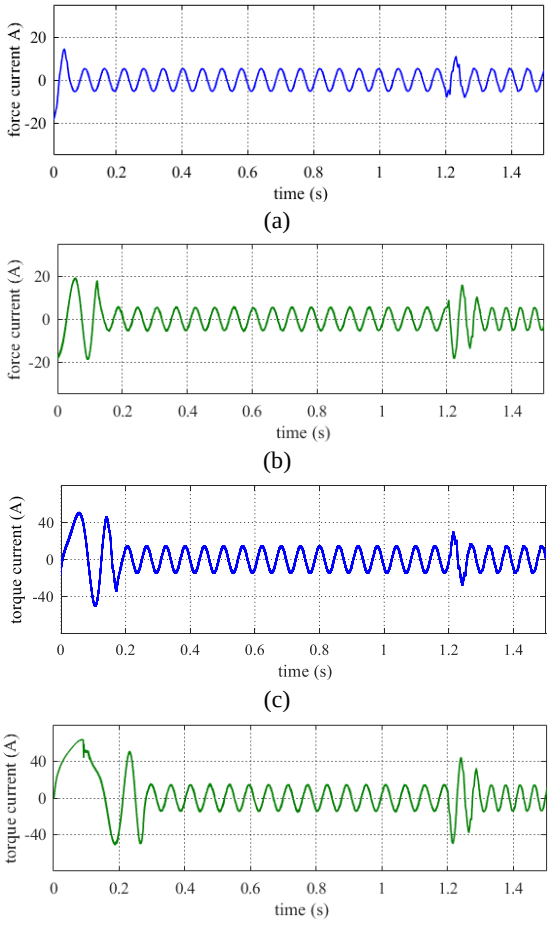

Fig. 11. Current comparison, (a) force current, proposed method, (b) force current, method presented in [20], (c) torque current, proposed method, (d) torque current, method presented in [20].

REFERENCES

[1] H. Azadrou, "Design and Optimization of a Very High Speed Three Phase Bearingless Induction Motor", International Journal of Industrial Electronics Control and Optimization, vol. 6, no. 4, pp. 283-289, 2023.

[2] T. Tera, Y. Yamauchi, A. Chiba, T. Fukao, and M. A. Rahman, "An improved mathematical model for speed sensorless control of fixed pole bearingless induction motor", *IEEE Trans. On Ind. Electronics*, vol. 71, no. 2, pp. 1286-1295, 2024.

[3] C. Lu, Z. Yang, X. Sun, Q. Ding, "Vibration compensation control strategy of composite cage rotor bearingless induction motor based on fuzzy coefficient adaptive-linear-neuron method", *ISA Transactions*, vol. 43, no. 1, pp. 66-77, 2024.

[4] S. Zhang, and F. L. Luo, "Direct control of radial displacement for bearingless permanent-magnet-type synchronous motors", *IEEE Trans. On Ind. Electronics*, vol. 56, no. 2, pp. 852-861, 2008.

[5] A. Chiba, D. Akamatsu, T. Fukao, and A. A. Rahman, "An improved rotor resistance identification method for magnetic field regulation in bearingless induction motor drives", *IEEE Trans. On Ind. Electronics*, vol. 55, no. 2, pp. 542-553, 2009.

[6] J. Huang, B. Li, H. Jiang, and M. Kang, "Analysis and control of multiphase permanent-magnet bearingless motor with a single set of half-coiled winding," *IEEE Trans. Ind. Electronics*, vol. 61, no. 7, pp. 3137–3145, 2014.

[7] H. Mitterhofer, B. Mrak, and W. Gruber, "Comparison of high-speed bearingless drive topologies with combined windings," *IEEE Trans. Ind. Applications*, vol. 51, no. 3, pp. 2116–2122, 2015.

[8] G. Sala, G. Valente, A. Formentini, and et al., "Space vectors and pseudoinverse matrix methods for the radial force control in bearingless multisector permanent magnet machines," *IEEE Trans. Ind. Electron*., vol. 65, no. 9, pp. 6912–6922, 2018.

[9] R. Oishi, S. Horima, H. Sugimoto, and A. Chiba, "A Novel Parallel Motor Winding Structure for Bearingless Motors", *IEEE Transactions on Magnetics*, vol. 49, no. 5, pp. 2287-2290, 2013.

[10] J. Chen, Y. Fujii, M. W. Johnson, A. Farhan, and E. L. Severson, "Optimal Design of the bearingless induction motor", *IEEE Trans. Ind. Applications*, vol. 57, no. 2, pp. 1375–1389, 2021.

[11] W. Gruber, and S. Silber, "Dual field-oriented control of bearingless motors with combined winding system", *2018 International Power Electronics Conference* (*IPEC-Niigata* 2018 *-ECCE Asia*), Oct. 2018.

[12] N. Turk, N. Bulic, W. Gruber, "Nonlinear control of a bearingless flux-switching slice motor with combined winding system", *IEEE/ASME Transactions on Mechatronics*, vol. 25, no. 1, pp. 152-163, 2019.

[13] Q. K. Jasim, M. Moanes, E. Ali, "Design of suspension control system for bearingless induction motor using fuzzy-I controller", *International Journal of Power Electronics and Drive System (IJPEDS)*, vol. 14, no. 2, pp. 771-780, 2023.

[14] Z. Yang, J. Jia, X. Sun, T. Xu, "A fuzzy-ELADRC method for a bearingless induction motor", *IEEE Trans. On Power Electronics*, vo. 37, no. 10, pp. 11803-11813, 2022.

[15] R. Havangi, M. Moredi, "PSO Based EKF Wheel-rail Adhesion Estimation", International Journal of Industrial Electronics Control and Optimization, vol. 6, no. 1, pp. 49-62, 2022.

[16] Y. Jiang, R. A. Torres, and E. L. Severson, "Current regulation in parallel combined winding bearingless motors", *IEEE Trans. On Ind. Applications*, vol. 55, no. 5, pp. 4800-4810, 2019.

[17] N. Petersen, A. Khamitov, T. Slininger, and E. L. Severson, "Machine design and precision current regulation for the parallel DPNV bearingless motor winding", *IEEE Trans. On Ind. Applications*, vol. 57, no. 6, pp. 7000-7011, 2021.

[18] Y. Su, Z. Yang, X. Sun, Z. Shen, "Direct torque control of bearingless induction motor based on super-twisting sliding mode control", *Journal of Control and Decision*, vol. 37, no. 11, pp. 13238-13249, 2024.

[19] D. Akamatu, A. Chiba, and T. Fukao, “A novel rotor resistance indentification in slip frequency controlled bearingless induction motors,” in Proc. 9th ISMB, Lexington, KY, Aug. 2004, CD-ROM.
[20] X. Ye, X. Tang, K. Xing, H. Wang, J. Yao, T. Zhang, “Repetitive control for vibration suppression of bearingless induction motor”, IEEE ACCESS, vol. 12, pp. 60532-60540, 2024.

Reza Ghanizadeh received the B.S. degree in electrical engineering from the Ardabil Branch, Islamic Azad University, Ardabil, Iran, in 2009, and the M.S. and Ph.D. degrees in electrical engineering from the University of Birjand, Birjand, Iran, in 2012 and 2017, respectively. He is currently an Assistant Professor with the Urmia Branch, Islamic Azad University, Urmia, Iran. His research interests include power quality, robust optimization, design of microgrid controllers, FACTS device and machine drives.

Hamed Azadrou was born in Salmas, Iran, in 1983. He received his B.S. degree in electrical engineering from Islamic Azad University, Abhar Branch, Abhar, Iran, and M.S. degree from Dezful Branch, Dezful, Iran, and PhD degree from Islamic Azad University, Urmia Branch, Urmia, Iran. He is a member of science in Islamic Azad University, Salmas Branch, Iran since 2012.